Understanding the Cooperative Interaction between Myosin II and Actin Crosslinkers Mediated by Actin Filaments during Mechanosensation

Tianzhi Luo, Krithika Mohan, Vasudha Srivastava, Yixin Ren, Pablo A. Iglesias, and Douglas N. Robinson

Supplemental Materials

Supplemental Methods, Analysis, and Discussion

Pharmacological modulation of F-actin levels and the corresponding myosin mechanosensory responses

We used latrunculin-A and jasplakinolide to adjust the F-actin level in *myoII* null cells expressing GFP-myosin II and determined the amount of F-actin by rhodamine-phalloidin staining. Cells were grown overnight in the presence of 0.2% DMSO on coverslips, and were then treated with 5 μM latrunculin-A or 2 μM jasplakinolide for 20 min. The cells were fixed with -20°C acetone for 3 min. on ice and blocked in 1X PBT (1X PBS, 0.05% Triton X-100 and 0.5% BSA). Samples were stained with 160 nM rhodamine-phalloidin for 1 hour, then washed 4-5 times with 1X PBT and mounted in 90% glycerol 1X PBS. For quantification of the actin levels, images were acquired on an Olympus IX81 microscope under identical imaging conditions. The fluorescence signals were measured for each cell and used as an indicator of the relative F-actin amount. More than 300 cells were counted per condition and the signals were normalized to the average of the 0.2% DMSO control. The cells were also imaged using a Zeiss 510 Meta confocal microscope to study the effects on the actin and myosin II distributions.

Latrunculin treatment reduced the F-actin levels to 40% of control while jasplakinolide treatment increased F-actin levels four-fold (Fig. S2A,B). Both drug treatments induced aggregations of F-actin and myosin II in the cortex, which lead to the structural non-uniformity as compared to untreated cells. In the MPA assays, only very low pressures could be applied to latrunculin-A-treated cells due to their extremely high deformability (higher pressures aspirated the entire cell into the micropipette, making measurements at these pressures impossible). No mechanosensitive accumulation was observed at these low pressures. In contrast, jasplakinolide treatment did not alter the mechanoresponsiveness as compared to control over a range of aspiration pressures (Fig. S2C).

The 2D kinetic Monte Carlo simulations reflect the 3D events

In the lattice kinetic Monte Carlo simulations, we used a 2D simulation box. However, the simulations reasonably mimic 3D events because the length of mesh size, the length that single myosin covers along actin filament, the binding and unbinding rates, and the diffusion coefficients are based on 3D structures and 3D measurements (1). As far as the diffusion in different dimensions is concerned, the mean square displacements of a random walk during time period Δt are $\langle \Delta x \rangle^2 = 4D\Delta t$ and $\langle \Delta x \rangle^2 = 6D\Delta t$ for 2D and 3D cases, respectively, and hence the mean square displacement differs only by a factor of 1.5 between the 2D and 3D cases. However, differences between these 2D and 3D scenarios could slightly alter the cluster size.

The mean-field approximation of E_s from statistical mechanics

We considered a one-dimensional actin filament with N binding sites for myosin and used periodic boundary conditions to mimic an infinitely long filament. The partition function Z of the system at each ϕ was calculated from 10^7 random samplings according to $Z = \sum_j g_j \exp\left(-H_j / k_B T\right)$, where g_j is the corresponding degeneracy of the same energy level and H is the energy of the system defined as $H = U - E_{binding}$. Here, U is the free energy of the system in the absence of the binding of myosin to actin and $E_{binding}$ is the binding energy of the system. Mathematically, U has the form of $U = NE_{site} + N\phi E_{myo}$, where $N\phi$ gives the number of myosins in the system, and E_{site} and E_{myo} are the energies for the single binding site and myosin, respectively. The binding energy of the system is simply the sum of the binding energy of each myosin-actin complex that has been defined in the KMC scheme, *i.e.*, $E_{binding} = \sum_i \left(E_i^0 + \Delta E_i\right)$ and $\Delta E_i = \sum_k E_s^k\left(x_{ik}\right)$ for $1 \le i \le N\phi$. The system energy H then depends on the coverage ϕ. The probability of the system at energy level H_j is $P_j\left(H_j\right) = \frac{1}{Z} g_j \exp\left(-H_j / k_B T\right)$ and the mean value of H is $\langle H \rangle = \sum_j P_j H_j$. It is noted that U and E_i^0 are constants for each $N\phi$ and do not depend on the permutation of the myosin positions. As a result, they cancel out eventually in the

exponential terms in both the numerator and the denominator of P_j. By expanding both sides of $\langle H \rangle = \sum_j P_j H_j$, one has

$$\left\langle U - \sum_i E_i^0 - \sum_i \Delta E_i \right\rangle = \frac{\sum_j g_j \left(U - \sum_i E_i^0 - \sum_i \Delta E_i \right)_j \exp\left(\left(\sum_i \Delta E_i \right)_j \Big/ k_B T \right)}{\sum_j g_j \exp\left(\left(\sum_i \Delta E_i \right)_j \Big/ k_B T \right)}. \qquad \text{(S1)}$$

Again, considering that U and E_i^0 are constants, Eq. S1 reduces to

$$\left\langle \sum_i \Delta E_i \right\rangle = \frac{\sum_j g_j \left(\sum_i \Delta E_i \right)_j \exp\left(\left(\sum_i \Delta E_i \right)_j \Big/ k_B T \right)}{\sum_j g_j \exp\left(\left(\sum_i \Delta E_i \right)_j \Big/ k_B T \right)}. \qquad \text{(S2)}$$

$\left\langle \sum_i \Delta E_i \right\rangle$ is the average change in the binding energy of the system due to the cooperative interactions. Since $\sum_i \Delta E_i = \sum_i E_s^i(x_{ik}) = \sum_i \sum_k E_s^0 \exp(-|x_{ik}|/\lambda)$, the mean-field approximation of $\sum_i \Delta E_i$, E_s, can be calculated exactly for each $N\phi$ using Eq. S2 and the values of E_s^0 and λ.

The effect of the distribution of actin filament length on the cooperativity of myosin II

The mesh size of actin network is an average distance between the crosslinking points. In 2D lattice kinetic Monte Carlo simulations, the window size of simulation box is equal to the mesh size assumed. When the mesh size is much larger than the characteristic decay length of the strain field, λ, changing the mesh size only affects the effective actin concentration in the simulation box and does not qualitatively change the cooperativity between bound myosins. However, in cells, the actin filament length has a broad distribution, varying from a few nanometers to submicron or even microns. If the length of certain actin filaments is close to the decay length, λ ($3a = 15$ nm), the cooperativity of myosins on these filaments will not be as strong as predicted (or simulated) by this paper. To compare the simulation results in this paper to the myosin behaviors in real cells, it is necessary to take the distribution of actin filament length into account. For WT *Dictyostelium* cells, the mean and the median of the actin filament length are 94 nm and 81 nm, respectively (2). Therefore, the effect of the randomness of actin

filament lengths is negligible when we compare the simulations to the experiments with *Dictyostelium* cells.

The possibility of the force-dependency of the on-rate, k_1

Here, the "off" rates k_{-1} is considered to be the primary force dependent term for two reasons. The first is that the *in vitro* assay in Ref. (3) indicates the cooperativity of myosin II is dependent on the isometric, actin-bound state of myosin II. The second is that the myosin actin-binding lifetime is force-dependent (4). These two findings strongly suggest that the "off" rates (or the binding lifetimes of myosin to actin) are force-dependent. However, it is possible that the strain energy also affects the "on" rates by altering the actin filament structure, promoting myosin binding. Numerically, we can simulate the cooperativity associated with the changes of the "on" rates. However, with limited experimental evidence for changes in the "on" rate due to forces and strains, the biological relevance of such simulations is unclear.

The dependence of $\Delta E_b'$ on m

According to Eq. 3 (main text), k_{-1} is an exponential function of $\Delta E_b'$, which is a function of the amount of bound myosin (m) and is described by

$$\Delta E_b' = \delta m + Fd/\alpha m . \qquad \text{(S3)}$$

The first term represents the strain energy and the second term is associated with the applied force. δ can have a value of either δ_1 or δ_2 depending on the amount of bound myosin m according to Eq. 3. $\delta_1 > \delta_2$ is always true since $\chi_1 > \chi_2$. $\Delta E_b'$ reaches its minimum when m is at its critical value $m_{cr} = \sqrt{\alpha Fd/\delta}$. δ_{cr} may be defined as $\delta_{cr} = Fd/\alpha m_{cr}^2$. When $\delta > \delta_{cr}$, $\Delta E_b'$ increases with m and otherwise decreases with m. As a result, k_{-1} decreases with m if $\delta > \delta_{cr}$ and increases with m if $\delta < \delta_{cr}$. We then considered the case where $\delta_1 > \delta_{cr} > \delta_2$. Two curves (dotted lines) describing $\Delta E_b'$ as a function of ϕ are shown in Fig. S6A with $\delta = \delta_1$ and $\delta = \delta_2$, respectively. It is easier to discuss the dependence of $\Delta E_b'$ on m instead of ϕ as m is related to ϕ by $\phi = 3m/C_{actin}$. During myosin assembly, E_s initially has a slope of δ_1 at ϕ and the slope changes to δ_2 as the number of bound myosin ϕ exceeds ϕ^*. The corresponding transient

behavior of $\Delta E_b'$ is schematically indicated by the solid curve in Fig. 3A. $\Delta E_b'$ as a function of ϕ at different Fd/α for E_s^0 at 1, 2, and 3k_BT are shown in Figs S6B-D, respectively.

The concentration of unbound myosin monomer during myosin transport

In cells, the local myosin concentration changes but the concentration of certain myosin forms might be constant. The mobile or diffusible unit of myosin in cell cortex is more likely to be the unbound myosin monomer (UMM). The cytoplasm can be considered as a reservoir of UMM and diffusion is able to quickly smooth the UMM gradient in the cytoplasm, which means the concentration of UMM is constant during the BTF assembly induced by local force. Therefore, to simulate the myosin accumulation and BTF assembly during mechanosensing without using real 3D geometry (results shown in Fig. 5), the concentration of UMM (M and $\overline{M}$) is kept constant.

The sensitivity of k_- and k_+ in the absence of force

The coefficient k_- may be evaluated numerically by fitting the simulation results to the observation that the BTF fraction is ~20%-50%. Here, k_- varied in the range 0.004-0.1 s^{-1} assuming $C_{myosin} = 3.4$ μM, $C_{actin} = 20.0$ μM, $E_s^0 = 1.0\,k_BT$, and $Fd = 0$ (Fig. S7A). It can be seen that high k_- leads to less assembled BTF. At $k_- = 0.1$ s^{-1}, the BTF concentration is maintained at 0.7 μM, ~20% of the total myosin. For the case of $E_s^0 > 1.0\,k_BT$, larger k_- is needed to set steady-state BTF at 0.7 μM (not shown).

As a proof of principle, k_+ is varied by adjusting C_{actin} in the range of 5-20 μM, assuming that $C_{myosin} = 3.4$ μM, $k_- = 0.1$ s^{-1}, $E_s^0 = 1.0$ k_BT, and $Fd = 0$ (Fig. S7B). It can be seen that the high F-actin does promote BTF assembly and the saturation concentration of actin is about six times the myosin concentration, which is consistent with the experimental observations (5). For different E_s^0, it is true that higher k_+ leads to more bound myosin, which can be seen by comparing Fig. S8A to S8B. In these simulations, the force term is zero and the myosin concentration is constant. Hence, the simulations reflect the conditions of *in vitro* BTF assembly.

Estimation of the Fd term for *Dictyostelium* cells during MPA measurements

During MPA measurements, the applied pressure is transmitted through the membrane and the membrane-cortex linkage to the actin cortex. Initially, myosin II concentration in the cortex, C_{myosin}, is 4 μM of which approximately half is in BTFs (6). Assuming the thickness of the cortex is ~0.5 μm, ~2000 myosins per μm^2 counteract the pressure applied externally on the plasma membrane. Each myosin has two heads and a 4.0 pN stall force. As a result, the upper bound of duty ratio, 0.06, gives a maximum stress of ~0.5 $nN/\mu m^2$ if all engaged myosins are stalled due to the applied force. This leads to a corresponding maximum value of Fd of ~280 k_BT where Fd is based on the total force/area ($nN/\mu m^2$).

The relation between Fd term and the applied pressure during MPA measurements

Besides myosin II, a number of other load bearing units exist in the actin cytoskeleton, including actin crosslinking proteins whose concentrations are also on the order of 1 μM. Because these proteins bear some of the load, only a fraction of the applied pressure is distributed on myosin. Based on measurements of the cortical tension in interphase wild type and *myoII* null cells (2), we estimate that myosin II contributes ~20% of the cortical tension. Thus, it is reasonable to assume that myosin II only bears ~20% of the pressure applied on interphase wild type *Dictyostelium* cells during MPA measurements. Further support for this idea comes from the observation that reducing interphase cortical tension by 3-fold in *racE* mutants reduces the mechanosensitive pressure-range of interphase cells by 3-5-fold (RacE controls the distribution of cortical actin crosslinking proteins) (7). Therefore, the range of 0~280 k_BT of Fd for myosin II roughly corresponds to 0~2.5 $nN/\mu m^2$ (*i.e.*, the maximum is five times ~0.5 $nN/\mu m^2$) of the applied pressure on the intact wild type cytoskeleton when the cortical myosin II concentration is 4 μM.

Solving the reaction-diffusion equations of myosin BTF assembly and myosin accumulation in 3D geometry by COMSOL

The multi-scale model describing the BTF assembly formation and myosin accumulation was implemented using COMSOL Multi-physics (COMSOL, Burlington, MA) version 4.2. The model was configured using a geometry drawn in "2D and 2D" axially symmetric space, to take advantage of symmetry. Subsequent results were displayed in full three dimensions. Each simulation was meshed using a physics controlled "Normal mesh." The reaction-diffusion

equations describing the model were solved using the Coefficient Form Partial Differential Equation (PDE) Interface found under the Mathematics branch of Physics Interfaces, along with a zero flux boundary condition. The system of PDEs were first solved at steady state using the Multifrontal Massively Parallel Sparse (MUMPS) direct solver and the resultant solution set was used as the initial condition for subsequent simulations. For simulating transient behavior the MUMPS direct solver along with a Backward Differentiation Formula (BDF) time stepping method was used. The time step for every computation was allowed to be chosen by the solver through the "Free" time-stepping option, but the maximum time-step chosen by the solver was fixed to 0.1s. The total simulation time was set to 200 s. For all the numerical simulations, COMSOL Multi-physics accepts volume concentrations (μM) in SI derived units, so all concentrations were converted to mol/m^3 by multiplying (or dividing) by 10^{-3}. For simplicity, the maximum size of BTF in the simulations is n=5 although it was found experimentally that n could be as large as 36. The cell diameter was 10 μm. The diameter of the pipette was 5 μm and the length of the cylindrical part was 2.5 μm (Fig. S10). A diffusion coefficient 0.2 μm^2 /s (1), was chosen for all myosin forms except for BTF_4 and BTF_5 for which the diffusion coefficient was set to zero. The thickness of the actin cortex is 500 nm. The change of k_{-1} due to applied force was only applied to the actin cortex in the tip region.

The reaction-diffusion equations in the simulations are

$$
\begin{aligned}
\frac{\partial C_M}{\partial t} &= D\frac{\partial^2 C_M}{\partial \vec{x}^2} + (k_{-1}C_{M^*} - k_1 C_M) + \left(k_+ C_{\overline{M}} - k_- C_M\right) \\
\frac{\partial C_{\overline{M}}}{\partial t} &= D\frac{\partial^2 C_{\overline{M}}}{\partial \vec{x}^2} + (k_1 C_{\overline{M}^*} - k_{-1}C_{\overline{M}}) - \left(k_+ C_{\overline{M}} - k_- C_M\right) \\
\frac{\partial C_{\overline{M}^*}}{\partial t} &= D\frac{\partial^2 C_{\overline{M}^*}}{\partial \vec{x}^2} + (k_{-1}C_{\overline{M}^*} - k_1 C_{\overline{M}}) - \left(k_+ C_{\overline{M}^*} - k_- C_{M^*}\right) \\
\frac{\partial C_{M^*}}{\partial t} &= D\frac{\partial^2 C_{M^*}}{\partial \vec{x}^2} + (k_1 C_M - k_{-1}C_{M^*}) + \left(k_+ C_{\overline{M}^*} - k_- C_{M^*}\right) - 2\left(k_2 {C_{M^*}}^2 - k_{-2}C_D\right) \\
\frac{\partial C_D}{\partial t} &= D\frac{\partial^2 C_D}{\partial \vec{x}^2} + (k_2 {C_M}^2 - k_{-2}C_D) - 2\left(k_3 {C_D}^2 - k_{-3}C_T\right) - \left(k_4 C_D C_T - k_{-4}C_{BTF_3}\right) \\
&\quad - \left(k_5 C_D C_{BTF_3} - k_{-5}C_{BTF_4}\right) - \left(k_5 C_D C_{BTF_4} - k_{-5}C_{BTF_5}\right) \\
\frac{\partial C_T}{\partial t} &= D\frac{\partial^2 C_T}{\partial \vec{x}^2} + (k_3 {C_D}^2 - k_{-3}C_T) - \left(k_4 C_D C_T - k_{-4}C_{BTF_3}\right) \\
\frac{\partial C_{BTF_4}}{\partial t} &= D\frac{\partial^2 C_{BTF_4}}{\partial \vec{x}^2} + (k_5 C_D C_{BTF_3} - k_{-5}C_{BTF_4}) - \left(k_5 C_D C_{BTF\,4} - k_{-5}C_{BTF_5}\right) \\
\frac{\partial C_{BTF_5}}{\partial t} &= D\frac{\partial^2 C_{BTF_5}}{\partial \vec{x}^2} + (k_5 C_D C_{BTF_4} - k_{-5}C_{BTF_5})
\end{aligned}
\quad , \qquad \text{(S4)}
$$

where C represents the concentration and the subscripts correspond to different components in the assembly scheme. Parameters and algorithm are listed in Tables S1 to S3.

Supplemental References

1. Uehara, R., G. Goshima, I. Mabuchi, R. D. Vale, J. A. Spudich, and E. R. Griffis. 2010. Determinants of myosin II cortical localization during cytokinesis. Curr. Biol. 20:1080-1085.
2. Reichl, E. M., Y. Ren, M. K. Morphew, M. Delannoy, J. C. Effler, K. D. Girard, S. Divi, P. A. Iglesias, S. C. Kuo, and D. N. Robinson. 2008. Interactions between myosin and actin crosslinkers control cytokinesis contractility dynamics and mechanics. Curr. Biol. 18:471 - 480.
3. Tokuraku, K., R. Kurogi, R. Toya, and T. Q. Uyeda. 2009. Novel mode of cooperative binding between myosin and Mg2+ -actin filaments in the presence of low concentrations of ATP. J. Mol. Biol. 386:149-162.
4. Veigel, C., J. E. Molloy, S. Schmitz, and J. Kendrick-Jones. 2003. Load-dependent kinetics of force production by smooth muscle myosin measured with optical tweezers. Nat. Cell Biol. 5:980-986.
5. Mahajan, R. K., K. T. Vaughan, J. A. Johns, and J. D. Pardee. 1989. Actin filaments mediate *Dictyostelium* myosin assembly in vitro. Proc. Natl. Acad. Sci. U.S.A. 86:6161-6165.
6. Surcel, A., Y.-S. Kee, T. Luo, and D. N. Robinson. 2010. Cytokinesis through biochemical-mechanical feedback loops. Semin. Cell Dev. Biol. 21:866-873.
7. Ren, Y., J. C. Effler, M. Norstrom, T. Luo, R. A. Firtel, P. A. Iglesias, R. S. Rock, and D. N. Robinson. 2009. Mechanosensing through cooperative interactions between myosin II and the actin crosslinker cortexillin I. Curr. Biol. 19:1421-1428.
8. Berlot, C. H., P. N. Devreotes, and J. A. Spudich. 1987. Chemoattractant-elicited increases in Dictyostelium myosin phosphorylation are due to changes in myosin localization and increases in kinase activity. J. Biol. Chem. 262:3918-3926.
9. Mahajan, R. K., and J. D. Pardee. 1996. Assembly mechanism of *Dictyostelium* myosin II: Regulation by K^+, Mg^{2+}, and actin filaments. Biochemistry 35:15504-15514.
10. Moores, S. L., and J. A. Spudich. 1998. Conditional loss-of-myosin-II-munction mutants reveal a position in the tail that Is critical for filament nucleation. Mol. Cell 1:1043-1050.
11. Yumura, S., M. Yoshida, V. Betapudi, L. S. Licate, Y. Iwadate, A. Nagasaki, T. Q. Uyeda, and T. T. Egelhoff. 2005. Multiple myosin II heavy chain kinases: roles in filament assembly control and proper cytokinesis in *Dictyostelium*. Mol. Biol. Cell 16:4256-4266.
12. Takcás, B., E. O'Neall-Hennessey, C. Hetényi, J. Kardos, A. G. Szent-Györgyi, and M. Kovács. 2011. Myosin cleft closure determines the energetics of the actomyosin interaction. FASEB J. 25:111-121.
13. Zhou, Q., Y.-S. Kee, C. C. Poirier, C. Jelinek, J. Osborne, S. Divi, A. Surcel, M. E. Will, U. S. Eggert, A. Müller-Taubenberger, P. A. Iglesias, R. J. Cotter, and D. N. Robinson. 2010. 14-3-3 coordinates microtubules, rac, and myosin II to control cell mechanics and cytokinesis. Curr. Biol. 20:1881-1889.

Table S1. Constants.

Parameter	Value	Conversion to SI derived units	Description	Reference
D	0.2 $\mu m^2/s$	2 $x10^{-13}$ m^2/s	Diffusion coefficient	(1)
k_+	0.05 s^{-1}	0.05 s^{-1}	Scheme, Fig. 1	(8)
k_{-1}^0	300 s^{-1}	300 s^{-1}	Scheme, Fig. 1: Rate controlling conversion from bound and unbound states of myosin monomers in the absence of force and homo-cooperativity	(9)
k_2	0.37 $\mu M^{-1}s^{-1}$	370 $m^3/mol \cdot s$	Scheme, Fig. 1	(10)
k_{-2}	0.01 s^{-1}	0.01 s^{-1}	Scheme, Fig. 1	Our estimate
k_3	0.0395 $\mu M^{-1}s^{-1}$	39.5 $m^3/mol \cdot s$	Scheme, Fig. 1	(10)
k_{-3}	0.045 s^{-1}	0.045 s^{-1}	Scheme, Fig. 1	(9)
k_4	1.25 $\mu M^{-1}s^{-1}$	1250 $m^3/mol \cdot s$	Scheme, Fig. 1	(9)
k_{-4}	0.025 s^{-1}	0.025 s^{-1}	Scheme, Fig. 1	(9)
k_5	10 $\mu M^{-1}s^{-1}$	10,000 $m^3/mol \cdot s$	Scheme, Fig. 1	Our estimate
k_{-5}	0.2 s^{-1} (for WT) or 0.005 s^{-1} (for 3xAla)	0.2 s^{-1} / 0.005 s^{-1}	Scheme, Fig. 1	(2, 11, 13)
k_{on}	0.45 $\mu M^{-1}s^{-1}$	450 $m^3/mol \cdot s$	On rate for myosin binding to actin	(12)
C_{actin}	72 μM	72 $x10^{-3}$ mol/m^3	Actin concentration in the cytosol	(6)
C_{actin_cortex}	79 μM	79 $x10^{-3}$ mol/m^3	Actin concentration in the cortex	(6)
$C_{myo\ total}$	3.4 μM	3.4 $x10^{-3}$ mol/m^3	Total cellular myosin II concentration	(6)
α	36 μM^{-1}	36 $x10^{-6}$ M^{-1}	The product of the duty ratio, a geometric factor and the Avogadro's number	(6)

Table S2. Variables.

Parameter	Method of evaluation	Description
$k_{\_}$	Evaluated numerically by fitting simulation results to the observation that $C_{\text{myo BTF}}$ = ~ 20-50% of $C_{\text{myo Total}}$ (ref.(13))	Scheme, Fig. 1: Myosin tail phosphorylation rate
k_1	$k_{on}C_{\text{actin}}$	Scheme, Fig. 1: Rate controlling conversion from bound and unbound states of myosin monomers
k_{-1}	$k_{-1}^{0}\exp(-\Delta E_b^{'}(x,y,t)/k_BT)$	Scheme, Fig. 1: Rate controlling conversion from bound and unbound states of myosin monomers

Table S3. Algorithm for calculating k_{-1}.

$k_{-1}(x,y,t) = k_{-1}^{0}\exp(-\Delta E_b^{'}(x,y,t)/k_B T)$	
$\Delta E_b^{'}(x,y,t) = E_s + \dfrac{Fd(\theta)}{\alpha m(x,y,t)}$	
$E_s = \begin{cases} \chi_1\varphi \\ \chi_1\varphi^* + \chi_2(\varphi - \varphi^*) \end{cases}$	where χ_1, χ_2, and φ^* are derived from Fig. S5C.
$\varphi = \dfrac{3m(x,y,t)}{C_{\text{actin}}}$	
$Fd(\theta) = Fd_0\cos(\theta)$	where $\cos(\theta) = \cos(\arctan(y,x))$, and Fd_0 is the energy associated with the maximum applied stress at the cortex by micropipette aspiration.
$m(x,y,t) = M^* + \overline{M}^* + 2D^* + 4T^* + \sum BTF_n^*$	

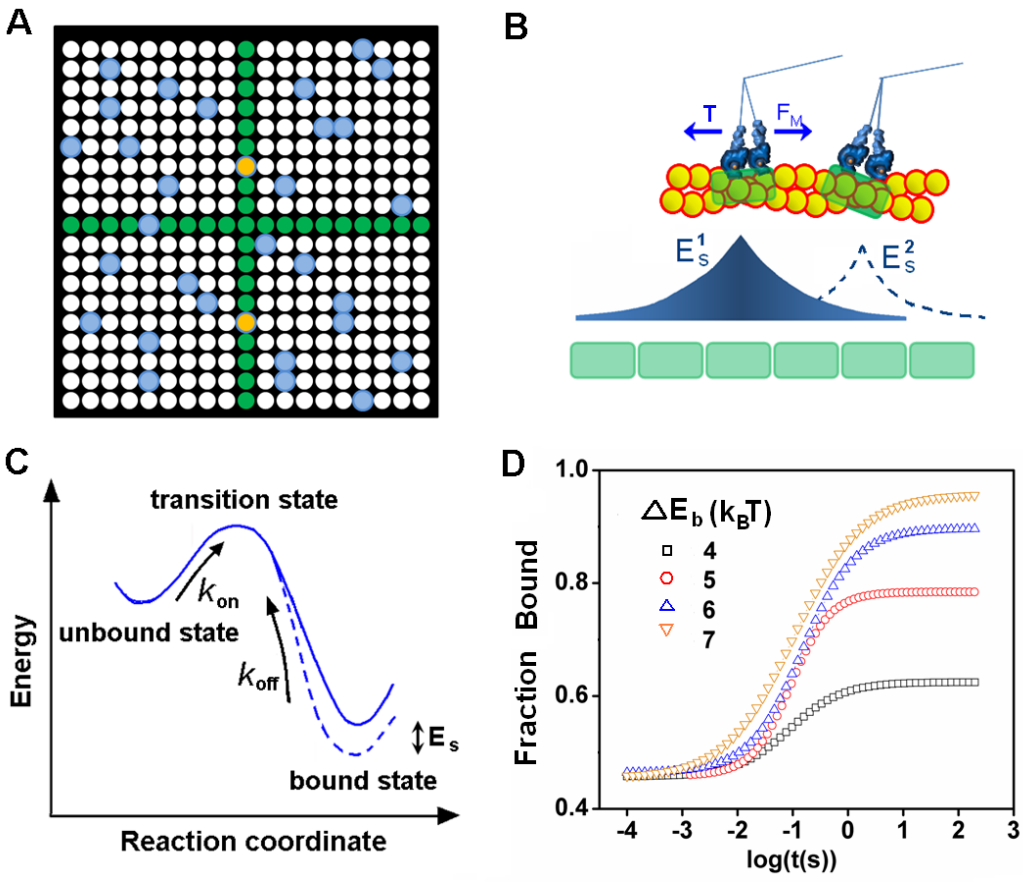

Figure S1. Kinetic Monte Carlo model for cooperative myosin binding to actin filaments. (A) A schematic graph of the 2D lattice for the KMC simulation is shown. White dots are empty lattices. Green dots are available binding sites. Yellow dots and blue dots represent bound and unbound myosins. (B) The exponentially decaying strain field associated with binding. The binding sites are indicated by green blocks. (C) The energy landscape of myosin binding to actin. E_s is the change of binding energy due to strain. (D) The kinetic binding curves of myosins for different changes of binding energy due to cooperative binding are shown.

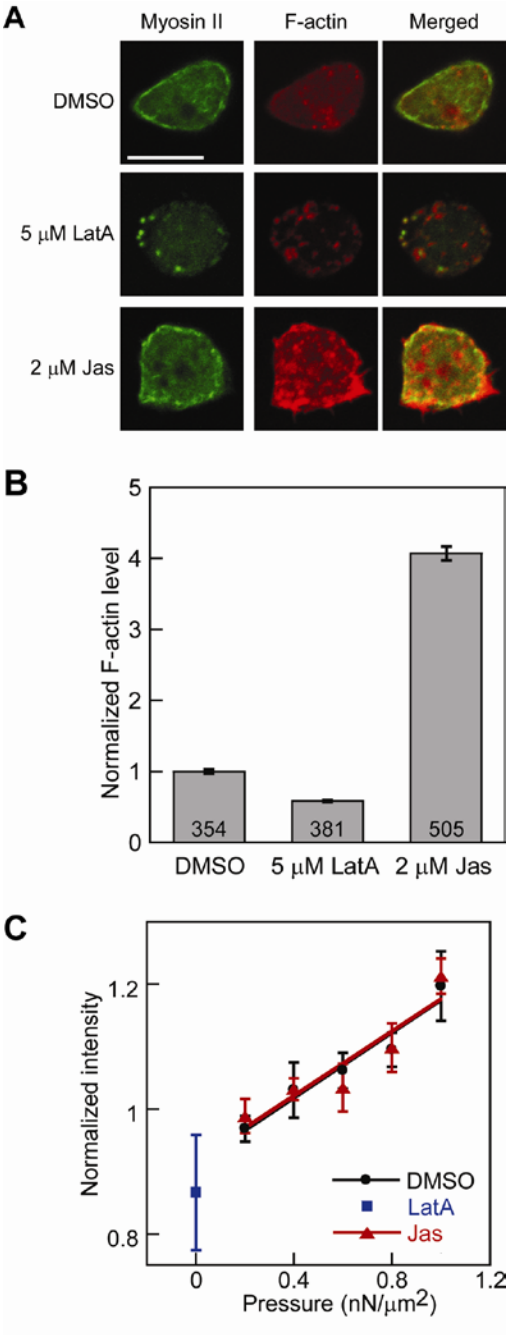

Figure S2. Adjustment of the myosin II cortical localization and its mechanosensory response using actin inhibitors. (A) Confocal images of GFP-myosin II and rhodamine-phalloidin stained F-actin in fixed cells treated by 5 μM latrunculin and 2 μM jasplakinolide. Scale bar represents 10 μm. (B) The quantified F-actin levels for different drug treatments (the number of cells measured per condition is listed on the histogram). (C) The mechanosensory response of myosin with different drug treatments at different pressures. At each pressure, the data point (mean±SEM) represents measurements from 15-20 cells.

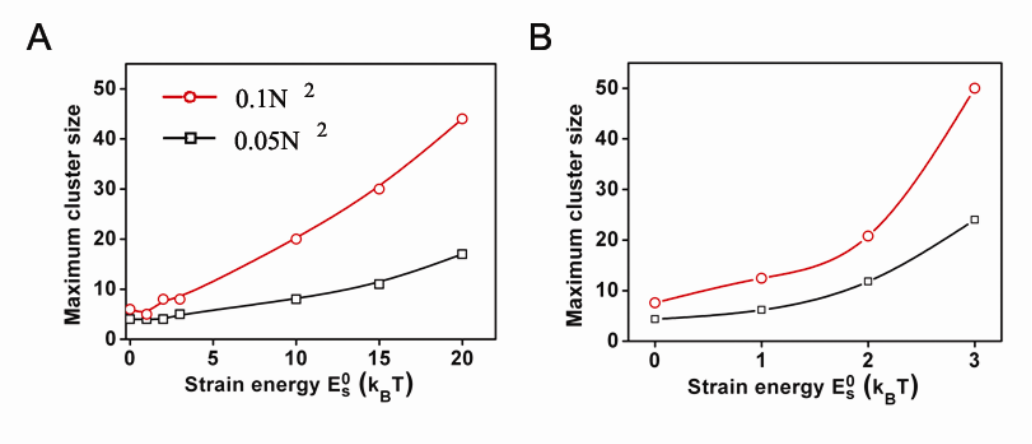

Figure S3. The nearest-neighbor interaction underestimates the effect of cooperativity on myosin binding to F-actin. The maximum cluster size of bound myosin in 2D lattice KMC simulations with nearest-neighbor interaction (*i.e.*, $|x_{ij}| = a$), and long-range interactions (for example, $|x_{ij}| \leq 3a$) are shown in (A) and (B), respectively. The myosin concentration is expressed in units of the simulation window size, N. Here, N=128, and the legend insert applies to both panels.

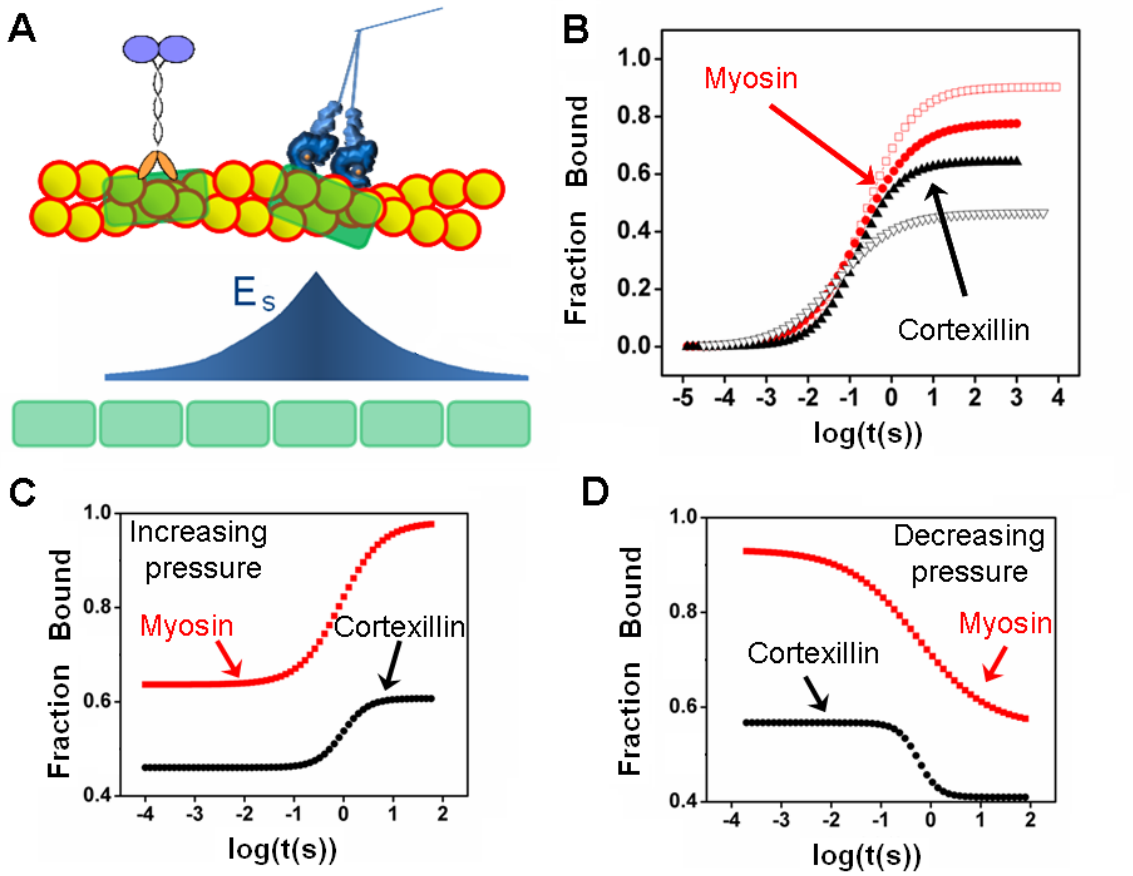

Figure S4. Kinetic Monte Carlo simulation of hetero-cooperative actin binding by myosin II and cortexillin I. (A) The strain field in the hetero-cooperative binding regime is shown. (B) Graph shows the binding curves of myosin alone (open red dots), cortexillin alone (open black triangles) and the mixture of myosin and cortexillin (the filled dots and filled triangles). (C) and (D) show the binding behaviors of the protein mixture in response to pressure jumps.

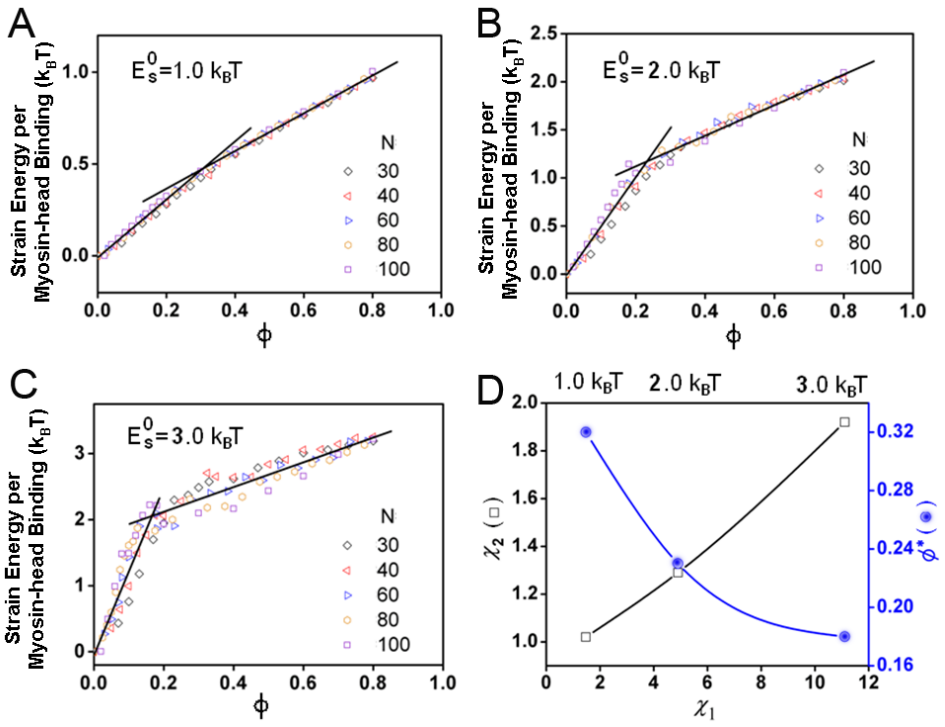

Figure S5. The mean-field approximation of strain energy per myosin-head binding. The change of binding energy is calculated from statistical mechanics for strain energy E_s^0 at 1 k_BT (A), 2 k_BT (B) and 3 k_BT (C) with different numbers of binding sites, N. Here, ϕ is the coverage of the actin filaments by the bound myosins. (D) The values of χ_1, χ_2 and ϕ^* at different strain energies (E_s^0 = 1, 2, 3 k_BT increasing from left to right).

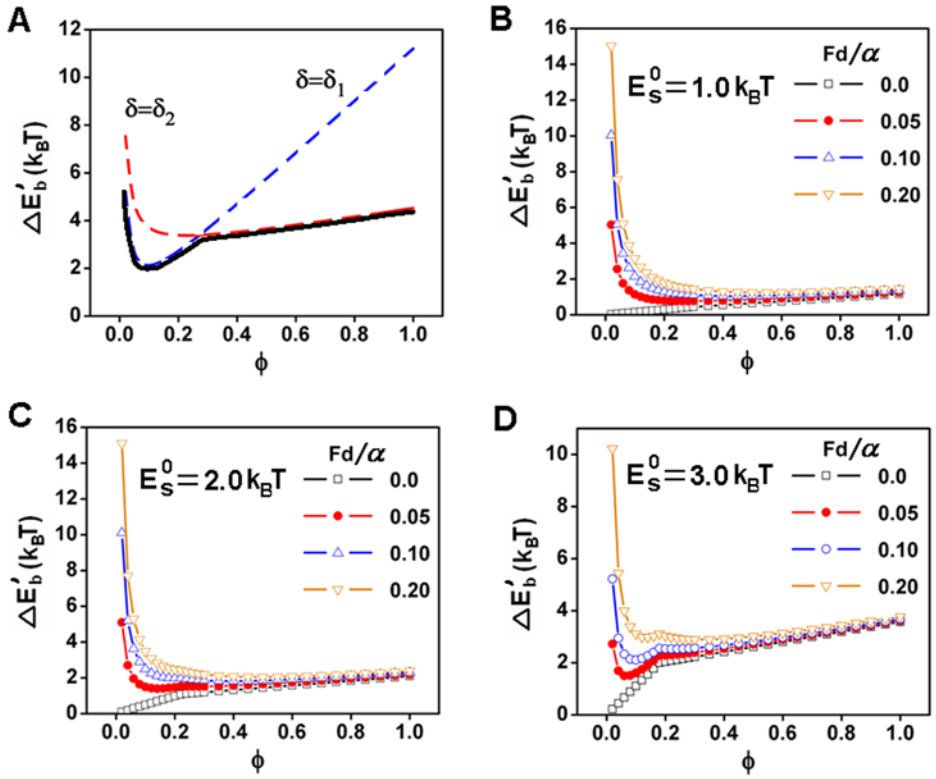

Figure S6. The dependence of $\Delta E_b'$ on m, the amount of bound myosin II. (A) A schematic plot shows how $\Delta E_b'$ (black solid line) changes its slope from δ_1 (blue dotted line) to δ_2 (red dotted line). The $\Delta E_b'$ changes as a function of m for different Fd/α when E_s^0 has a value of 1.0 k_BT (B), 2.0 k_BT (C) and 3.0 k_BT (D).

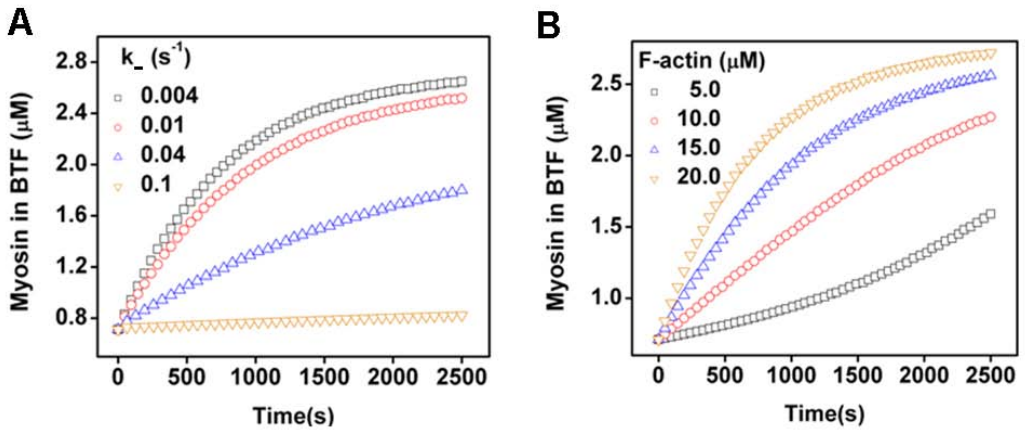

Figure S7. The kinetics of *in vitro* BTF assembly. (A) The assembly kinetics are shown for a fixed actin concentration but with different $k_{\_}$. (B) The assembly kinetics are shown for different F-actin concentrations for $E_s^{\,0}$ at 1.0 $k_{\mathrm{B}}T$.

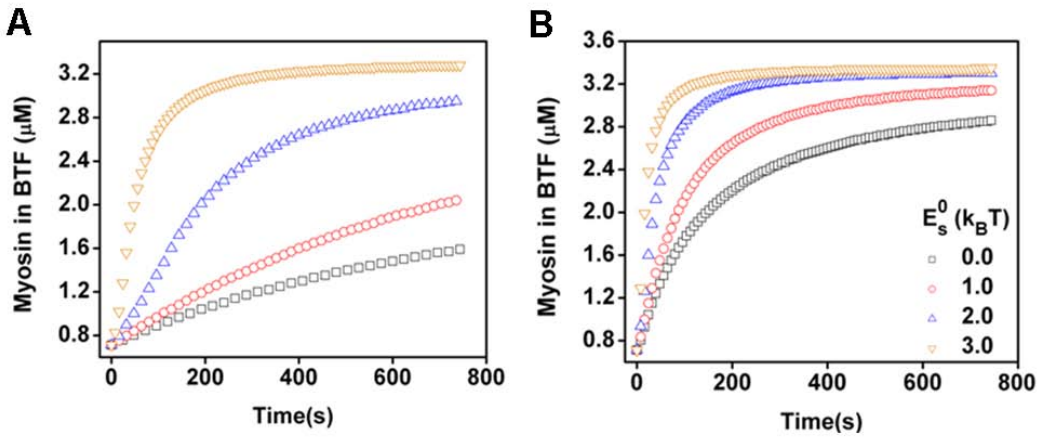

Figure S8. The myosin BTF assembly for k_+ at 6.6 s^{-1} (A) and 66.0 s^{-1} (B), respectively. For all cases $C_{myosin} = 3.4$ μM, $C_{actin} = 20.0$ μM, and $Fd = 0\ k_BT$.

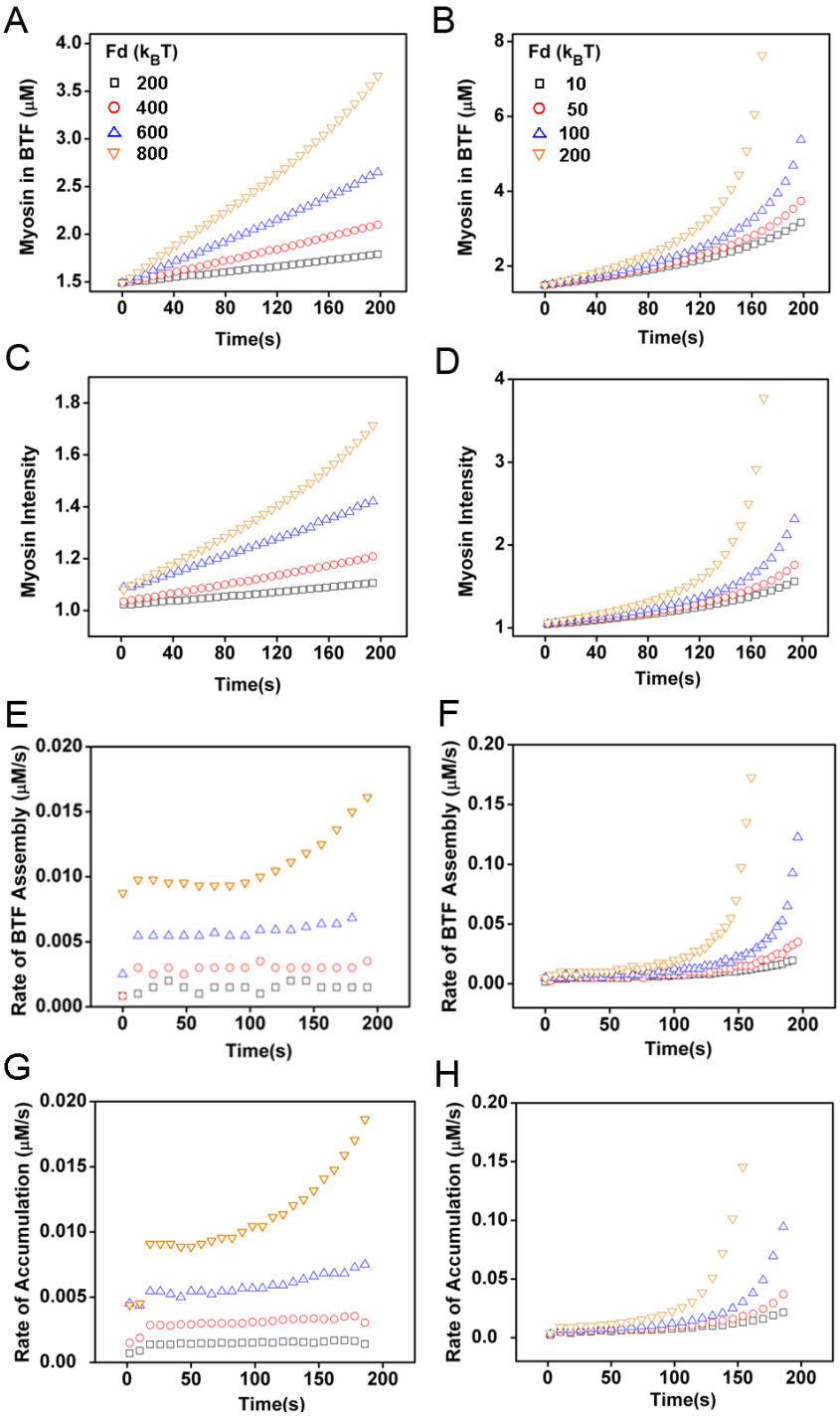

Figure S9. The BTF assembly, the associated myosin intensity and the corresponding rates are calculated at different Fd **values but with same cooperativity,** $E_s^0 = 3\ k_BT$**.** Left column is for k_1: 7 s^{-1} whereas right column is for k_1: 14 s^{-1}.

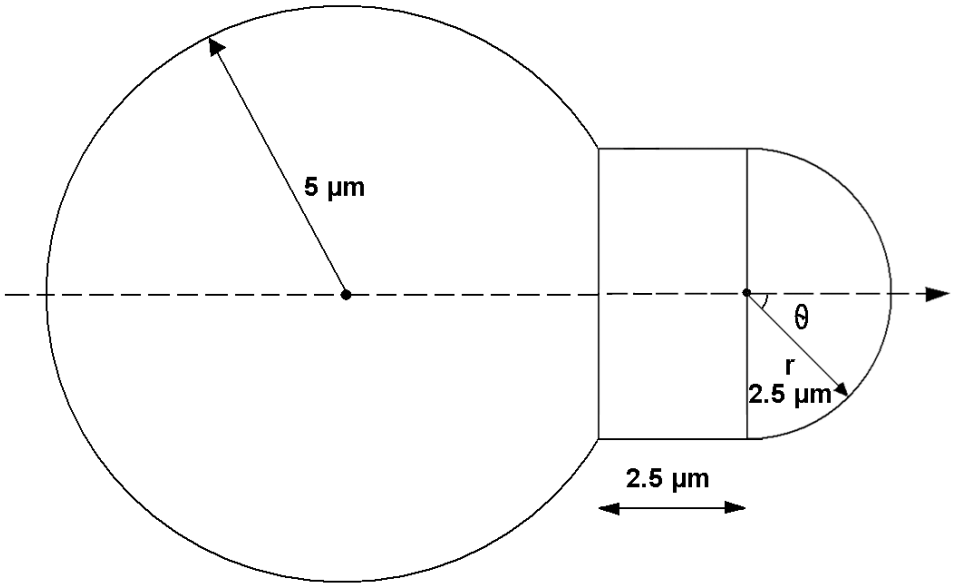

Figure S10. The geometry of the cross-section of the cell region aspirated into the micropipette used for 3D simulations in COMSOL.

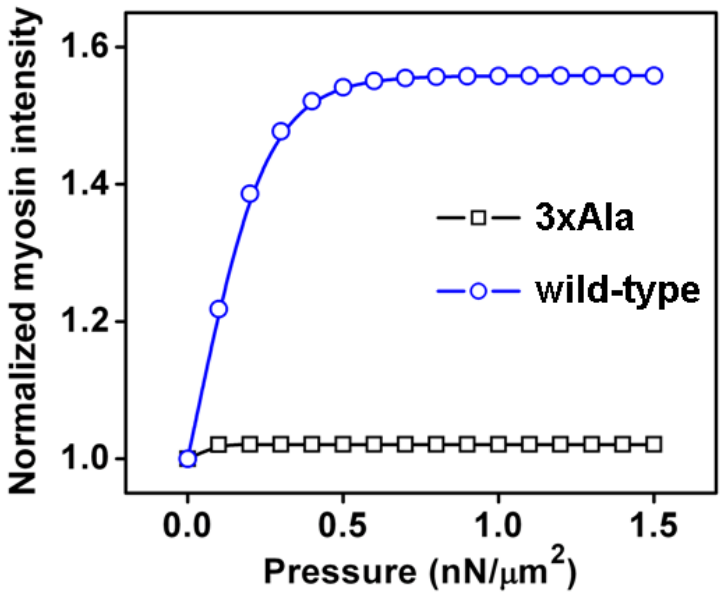

Figure S11. The normalized myosin intensity increased with the applied pressure, ΔP. Here, the force-dependent term in Eq. 3, $Fd/\alpha m$, is rewritten as $\Delta P \Delta A d/(2\rho \Delta A h N_A m)$, where area $\Delta A = 1\,\mu m^2$, duty ratio $\rho = 0.06$, thickness of cell cortex h = 0.5 μm and N_A is the Avogadro's number.

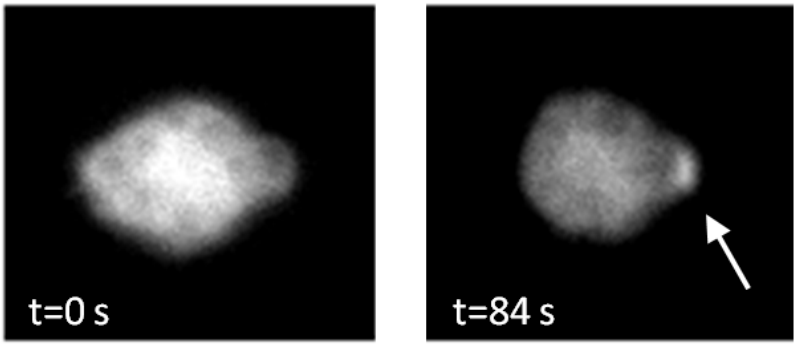

Figure S12. The accumulation of myosin heavy chain kinase C in response to pressure at different time frames.

Supplemental Movie Legends

Supplemental Movie 1. Movie shows the simulation result for cooperative binding of myosin II to actin filaments. The bound myosins (orange dots) form clusters on the actin filaments. The grey dots are the freely diffusing monomers. The time delays between each frame increase logarithmically.

Supplemental Movie 2. Movie shows the simulation result for cooperative binding of myosin II and cortexillin I. Clusters containing both myosin II and cortexillin I are formed due to hetero-cooperativity. The bound myosins and cortexillins are represented by yellow and red dots, respectively. The unbound myosins and cortexillins are represented by grey and green dots, respectively. The time delays between each frame increase logarithmically.

Supplemental Movie 3. Movie shows the accumulation of WT myosin II in response to applied force.

Supplemental Movie 4. Movie shows the accumulation of 3xAla myosin II in response to applied force.

Supplemental Movie 5. Movie shows a 3D view of WT myosin II accumulation in response to applied stress. The movie has an 85° cutout so that the cell interior is visible.